Numerical Study of Shock-Cylinder Banks Interactions

S. P. Wang, M. Anderson, J. Oakley and R. Bonazza
Department of Engineering Physics, University of Wisconsin-Madison,
Madison, WI 53706

Introduction

Designs of inertial fusion reactor chambers, such as the LIBRA-SP, utilize rows of cooling tubes to absorb energy from the fusion reaction as well as target debris. The reaction also results in a hydrodynamic shock wave in the low pressure blanket gas that spherically radiates from the center of the chamber out to the rows of cooling tubes. A shock tube has been used to model experimentally the interaction of a shock wave with two rows of cooling tubes. The shock tube studies have been repeated in a computational environment and the numerical results compare favorably with the experiments. The numerical studies are now extended to a bank of cylinders, consisting of five rows, with the goal of understanding the most favorable geometrical spacing of the cooling tubes for structural design purposes.

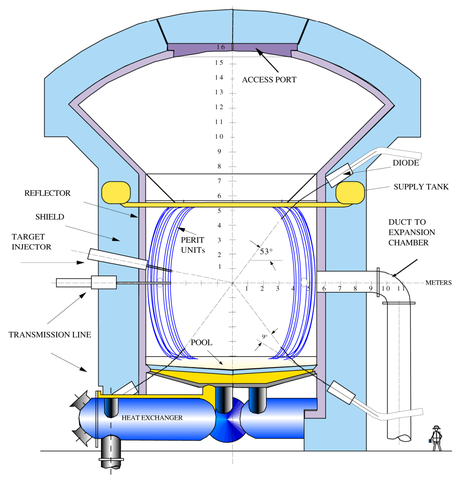

Cross-Section of the LIBRA-SP Target Chamber

Wisconsin Shock Tube Laboratory

- Vertical Orientation
- Large Internal Square
- Cross-Section (25 cm square)
- Total Length=9.3 m
- Driven Length=6.8 m
- Structural Capacity 20 MPa
- Modular Construction

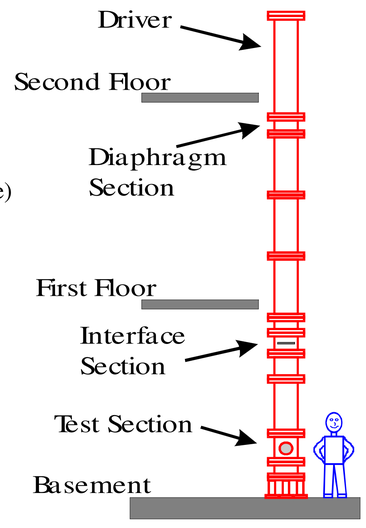

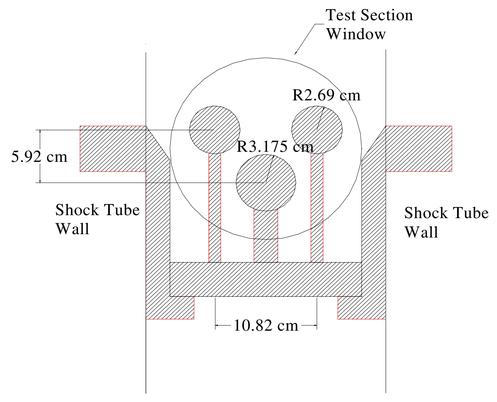

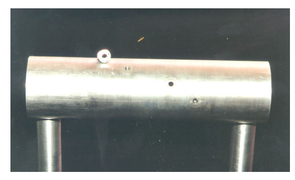

Cylinders used to model cooling tubes have flush mounted pressure transducers every 30 degrees around the circumference.

Key Features of the Numerical Code

The code solves the Euler equations in two-dimensions using an exact Riemann solver and a fourth-order accurate (spatial) piece-wise spline method (PSM). The Euler equations in conservative form are:

$$\mathbf{U}_t + \mathbf{F}(\mathbf{U})_x + \mathbf{G}(\mathbf{U})_y = 0 \qquad (1)$$

where the conservative variables (**U**) and fluxes (**F** and **G**) are:

$$\mathbf{U} = \begin{pmatrix} \rho \\ \rho u \\ \rho v \\ E \end{pmatrix}; \mathbf{F} = \begin{pmatrix} \rho u \\ \rho u^2 + p \\ \rho uv \\ u(E+p) \end{pmatrix}; \mathbf{G} = \begin{pmatrix} \rho v \\ \rho uv \\ \rho v^2 + p \\ v(E+p) \end{pmatrix} \qquad (2)$$

The total energy per unit volume is $E = \rho\left(1/2\left(u^2 + v^2\right) + e\right)$ and the calorically perfect gas model is used:

$$e = p/\rho(\gamma - 1)$$

A splitting scheme is employed for the system in two spatial dimensions and the tangential velocity component, v(u) in the x-sweep(y-sweep), is passively advected with the normal velocity component, u(v). A two-step process shown is used to accomplish the integration from time n to n+1 using a Godunov scheme:

$$\mathbf{U}_{i,j}^{n+1/2} = \mathbf{U}_{i,j}^{n} + \frac{\Delta t}{\Delta x}\left(\mathbf{F}_{i-1/2,j}^{n} - \mathbf{F}_{i+1/2,j}^{n}\right); \ \forall j \qquad (3)$$

$$\mathbf{U}_{i,j}^{n+1} = \mathbf{U}_{i,j}^{n+1/2} + \frac{\Delta t}{\Delta y}\left(\mathbf{G}_{i,j-1/2}^{n+1/2} - \mathbf{G}_{i,j+1/2}^{n+1/2}\right); \ \forall i \qquad (4)$$

The PSM and following slope limiters, similar to those developed by Ren et al. (1996), are used for the data reconstruction of the conservative variables for the local Riemann problem solutions at cell interfaces to achieve fourth order (spatial) accuracy:

$$\mathbf{U}_i^L = \mathbf{U}_i^n - \frac{\Delta x_i}{2}\mathbf{m}_i + \frac{(\Delta x_i)^2}{8}\mathbf{M}_i - \frac{(\Delta x_i)^3}{48}\mathbf{M}_i^{(3)} \qquad (a)$$

$$\mathbf{U}_i^R = \mathbf{U}_i^n + \frac{\Delta x_i}{2}\mathbf{m}_i + \frac{(\Delta x_i)^2}{8}\mathbf{M}_i + \frac{(\Delta x_i)^3}{48}\mathbf{M}_i^{(3)} \qquad (b)$$

$$\mathbf{U}_i^L = \mathbf{U}_i^n - \frac{1}{2}\min\text{mod}\left(\mathbf{m}_{i-1}, \mathbf{m}_i, \mathbf{m}_{i+1}\right)\Delta x_i + \frac{1}{8}\min\text{mod}\left(\mathbf{M}_{i-1}, \mathbf{M}_i, \mathbf{M}_{i+1}\right)(\Delta x_i)^2 - \frac{1}{48}\min\text{mod}\left(\mathbf{M}_{i-1}^{(3)}, \mathbf{M}_i^{(3)}, \mathbf{M}_{i+1}^{(3)}\right)(\Delta x_i)^3$$

$$\mathbf{U}_i^R = \mathbf{U}_i^n + \frac{1}{2}\min\text{mod}\left(\mathbf{m}_{i-1}, \mathbf{m}_i, \mathbf{m}_{i+1}\right)\Delta x_i + \frac{1}{8}\min\text{mod}\left(\mathbf{M}_{i-1}, \mathbf{M}_i, \mathbf{M}_{i+1}\right)(\Delta x_i)^2 + \frac{1}{48}\min\text{mod}\left(\mathbf{M}_{i-1}^{(3)}, \mathbf{M}_i^{(3)}, \mathbf{M}_{i+1}^{(3)}\right)(\Delta x_i)^3$$

and

$$\min\text{mod}\left(g_{i-1}, g_i, g_{i+1}\right) = \begin{cases} \min\left(|g_{i-1}|, |g_i|, |g_{i+1}|\right) sign\left(g_i\right) & \text{if } \min\left(g_{i-1}, g_i, g_{i+1}\right) \times \max\left(g_{i-1}, g_i, g_{i+1}\right) > 0 \\ 0 & \text{else} \end{cases}$$

where *m*, *M* and $M^{(3)}$ are the first, second and third derivatives of the conserved variable. The reconstructed variables are used with the Pike exact Riemann solver to evaluate the flux terms at the interface.

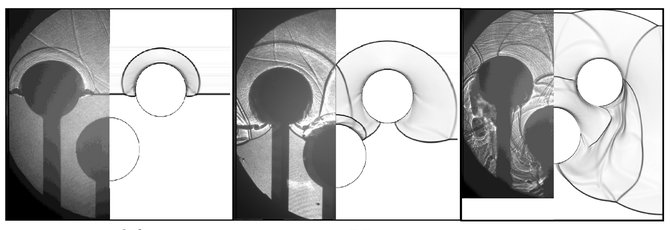

t_{image}≈36 μs t_{image}≈77 μs t_{image}≈191 μs

Shadowgraph shock diffraction patterns comparing experimental results (left) with numerical results (right) for a *M*=2.75 shock in atmospheric pressure argon. The shock is traveling from the top to the bottom and time zero is taken as the time when the shock is incident on the upper row of cylinders. Diffraction patterns compare favorably for the first two times but discrepancies arise in the later time image due to viscous effects and the effect of the cylinder support structure.

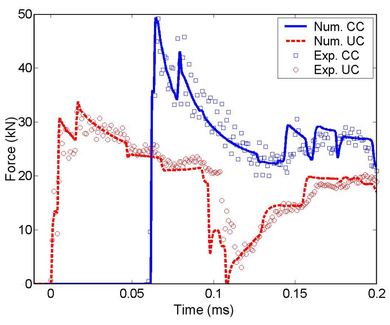

The vertical forces on the upper cylinder (UC) and lower, center cylinder (CC) are determined by integrating the pressure traces (taken at the discrete angular locations) around the cylinder. The shock is strengthened as it passes through the gap between the two upper cylinders resulting in a higher vertical force on the center cylinder. The numerical results compare favorably with the experimental, allowing for further numerical studies in regimes that can't be studied experimentally with the current shock tube.

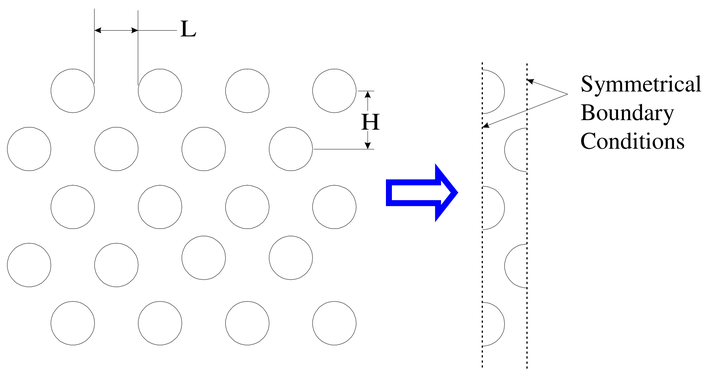

An infinite array of five rows of cooling tubes is numerically modeled as five rows of half-cylinders with symmetrical boundary conditions at the sides of the domain. The pitch ratio is defined as δ=L/H. The cylinders are modeled with reflective boundary conditions. The domain is 0.49 m in length and the spatial resolution is Δ*x*=Δ*y*=0.25 mm.

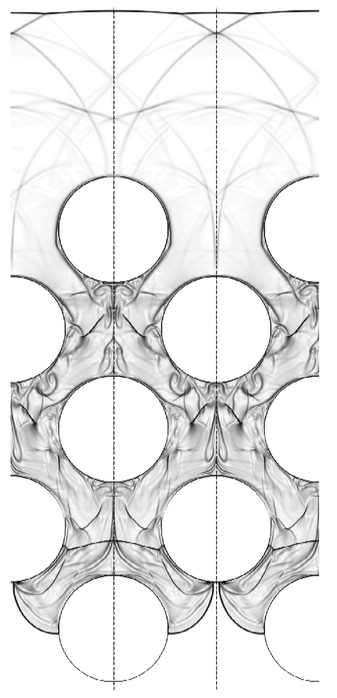

A numerical shadowgraph image when the shock has reached the midpoint of the fifth row of cylinders.

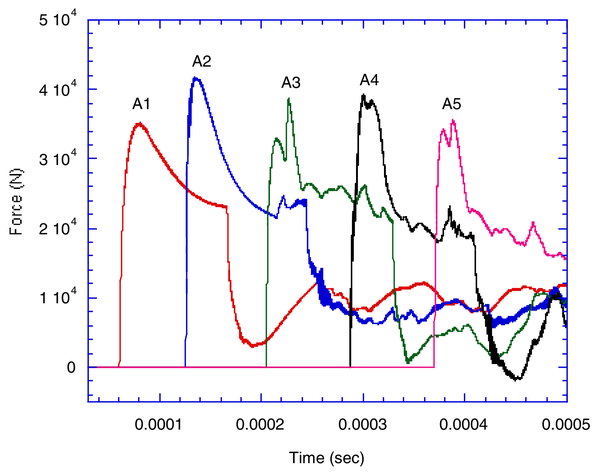

Test A: δ=1.0; *R*=2.95 cm; *H*=5.9 cm.

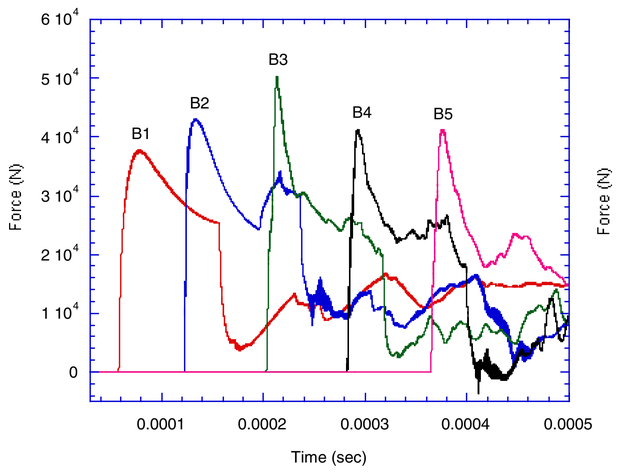

Test B: δ=0.924; *R*=3.175 cm; *H*=5.9 cm.

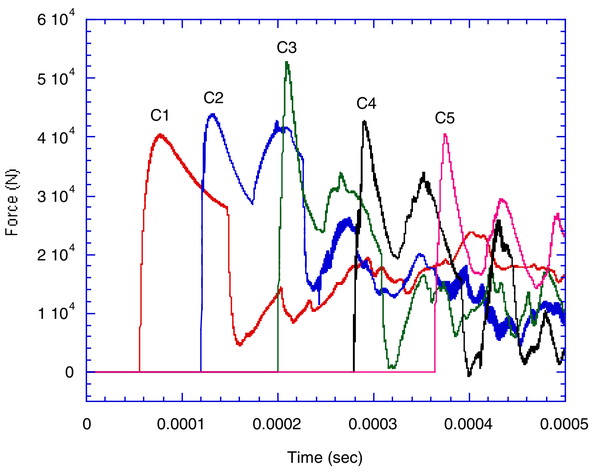

Test C: δ=0.849; *R*=3.395 cm; *H*=5.9 cm.

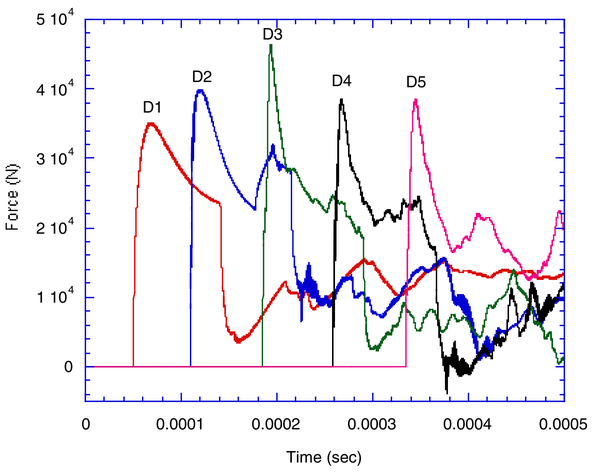

Test D: δ=0.924; *R*=2.95 cm; *H*=5.48 cm.

Case	R (cm)	H (cm)	L (cm)	δ
A	2.95	5.90	5.90	1
B	3.18	5.90	5.45	0.92
C	3.40	5.90	5.01	0.85
D	2.95	5.48	5.06	0.92

The vertical force is calculated using the following equation where *W* is the length of the cylinder:

$$F = 2\int_0^{\pi} P(\theta) R \sin(\theta) W d\theta$$

Results and Discussion

Four test cases, A-D, are presented with vertical force traces on each of the five rows of cylinders for a *M*=2.75 shock in argon. In each of the plots, the uppermost cylinder is labeled 1 while the lowermost is 5. It is seen from the force plots that the geometry of the cylinder placement has a strong effect on the maximum force on the cylinders. In case A the maximum force occurs on the second bank of cylinders while for cases B, C and D the maximum force occurs on the third row of cylinders. The maximum force seen in all of the simulations is for the third row of cylinders in case C which is most likely due to the fact that the radius of each cylinder is largest in this case. In all cases, the first cylinder bank is subjected to the lowest vertical force loading due to the shock strengthening that occurs as the shock wave traverses the gaps between the cylinders. The shock strengthening effect is seen to lessen as the shock reaches the fourth and fifth rows of cylinders due to the numerous shock reflections that have occurred by this later time. For the actual cooling tubes in an IFE reaction chamber it will be necessary to consider the force loading on each row in the structural design, that is, if the geometry of case A is used then the second row will have to be stronger than the others, while in cases B-D, the third row of tubes would require the highest strength.